HHS Public Access

Author manuscript

J Mol Med (Berl). Author manuscript; available in PMC 2020 July 01.

Published in final edited form as:

J Mol Med (Berl). 2019 July ; 97(7): 1033–1047. doi:10.1007/s00109-019-01791-z.

Therapeutic Potential of AAV9-S15D-RLC Gene Delivery in Humanized *MYL2* Mouse Model of HCM

Sunil Yadav[†], **Chen-Ching Yuan**[†], **Katarzyna Kazmierczak**[†], **Jingsheng Liang**[†], **Wenrui Huang**[†], **Lauro M. Takeuchi**[†], **Rosemeire M. Kanashiro-Takeuchi**[†], and **Danuta Szczesna-Cordary**[†,*]

[†]Department of Molecular and Cellular Pharmacology, University of Miami Miller School of Medicine, Miami, FL 33136, USA

Abstract

Familial hypertrophic cardiomyopathy (HCM) is an autosomal dominant disorder characterized by ventricular hypertrophy, myofibrillar disarray and fibrosis, and is primarily caused by mutations in sarcomeric genes. With no definitive cure for HCM, there is an urgent need for the development of novel preventive and reparative therapies. This study is focused on Aspartic acid-to-Valine (D166V) mutation in the myosin regulatory light chain, RLC (*MYL2* gene), associated with a malignant form of HCM. Since myosin RLC phosphorylation is critical for normal cardiac function, we aimed to exploit this post-translational modification via phosphomimetic-RLC gene therapy. We hypothesized that mimicking/modulating cardiac RLC phosphorylation in non-phosphorylatable D166V myocardium would improve heart function of HCM-D166V mice. Adeno-Associated Virus, serotype-9 (AAV9) was used to deliver phosphomimetic human RLC variant with Serine-to-Aspartic acid substitution at Ser15-RLC phosphorylation site (S15D-RLC) into the hearts of humanized HCM-D166V mice. Improvement of heart function was monitored by echocardiography, invasive hemodynamics (PV-loops) and muscle contractile mechanics. A significant increase in cardiac output and stroke work and a decrease in relaxation constant, Tau, shown to be prolonged in HCM mice, were observed in AAV- vs. PBS-injected HCM mice. Strain analysis showed enhanced myocardial longitudinal shortening in AAV-treated vs. control mice. In addition, increased maximal contractile force was observed in skinned papillary muscles from AAV-injected HCM hearts. Our data suggest that myosin RLC phosphorylation may have important translational implications for the treatment of RLC-induced HCM and possibly play a role in other disease settings accompanied by depressed Ser15-RLC phosphorylation.

[*]**Corresponding author:** Danuta Szczesna-Cordary, dszczesna@med.miami.edu. Phone: 305-2432908; FAX: 305-2434555.

Author Contributions: SY, CCY, WH, KK and DSC conceived research; SY, CCY, WH, KK, JL, LT, and RKT performed experiments; SY, CCY, KK, RKT and DS-C analyzed data; SY and DS-C wrote the paper.

Keywords

Adeno-associated virus; D166V-mutation; *in vivo* rescue of function; regulatory light chain (RLC); S15D-phosphorylation mimic

Introduction

Hypertrophic cardiomyopathy (HCM) is a complex, autosomal dominant disorder of cardiomyocytes with a prevalence over 1:500, marked by left ventricular (LV) and septal hypertrophy in the absence of increased external load, myofibrillar disarray and myocardial fibrosis, with increased risk for sudden cardiac death (SCD), heart failure (HF) and cardioembolic stroke [1–3]. Familial HCM is caused by mutations in genes encoding major sarcomeric contractile proteins such as β-myosin heavy chain (β-MHC), myosin regulatory (RLC) and essential (ELC) light chains, myosin binding protein C (MyBP-C), α-tropomyosin (α-Tm), troponin T (TnT), troponin I (TnI), troponin C (TnC), α-actin, and titin [4, 5]. At present, there is no cure for HCM, and symptomatic interventions rely on drugs that are often intended for broader cardiovascular disorders. Treatment options include implantable cardioverter-defibrillators for prevention of SCD, surgical myectomy (or alternatively, alcohol septal ablation) for treatment of HF symptoms by abolishing outflow tract obstruction, transcatheter ablation for atrial fibrillation and application of drugs [6]. In spite of these strategies that have resulted in a lower disease-related mortality, HCM still remains a sector with unmet need and research priority, and any effective pharmacological therapy must effectively and specifically target the underlying mechanisms involved in the pathogenesis of the disease.

Myosin RLC is a major regulatory subunit of striated muscle contraction and a modulator of the troponin and Ca^{2+}-controlled development of force and sarcomere shortening [7]. It is localized at the head-rod junction of the myosin heavy chain and, along with the essential light chain, stabilizes the α-helical neck of the myosin head [8]. In addition to the N-terminal divalent Ca^{2+}-Mg^{2+} binding site, RLC contains a functionally important myosin light chain kinase (MLCK)-specific phosphorylation site at Ser-15 [4, 9]. A plethora of research studies recognize the role of Ser-15 phosphorylation in cardiac muscle contraction, playing crucial role in the function of the heart under normal and disease conditions (reviewed in [10]). Significantly depressed levels of RLC phosphorylation have been observed in HF patients [11, 12], and were also reported in experimental animal models of cardiac disease [13–16]. Studies in mice have further revealed that reduced RLC phosphorylation coincides with abnormal heart performance, through morphological and/or myofibrillar functional alterations [13, 17–19].

Genetic studies have revealed numerous mutations in *MYL2*, encoding the human ventricular RLC, as causative mutations in hypertrophic cardiomyopathy (reviewed in [4, 20]). This study is focused on D166V (Aspartic acid-to-Valine) mutation, found by Richard et al. [21] in HCM patients and implicated with malignant HCM phenotype. Using transgenic D166V mice, we previously demonstrated a mutation-specific functional change in Ca^{2+}-dependent myocardial contraction that coincided with a significant decrease in the

endogenous level of RLC phosphorylation [13]. We suggested that a mutation-induced disruption at the phosphorylatable Ser-15 RLC site may trigger a series of biochemical perturbations and lead to altered actin-myosin interactions via D166V-induced inhibition of the MLCK-specific phosphorylation of RLC. Interestingly, MLCK-induced phosphorylation of transgenic D166V cardiac muscle preparations was sufficient to partially rescue the negative functional consequences of the D166V mutation assessed in myofibrils as well as in skinned papillary muscle strips [22]. We also previously explored a novel rescue mechanism via constitutive RLC phosphorylation, using pseudo-phosphorylated RLC mimetic recombinant proteins containing the S15D or S15A (Ser-15 replaced by Aspartic acid/Alanine) in the background of HCM-D166V mutation and reconstituted in porcine cardiac muscle preparations [23]. The S15D-induced rescue of V_{max} of the actin-activated myosin ATPase activity and an increase in force production capability were observed in the *in vitro* motility assays and in skinned papillary muscle fibers reconstituted with S15D-D166V compared with D166V alone or S15A-D166V [23]. These *in vitro* studies suggested that RLC phosphorylation may counteract the effects of D166V via phosphorylation-induced RLC conformation change rather than the enzymatic activity of the MLCK or phosphatase and prompted our *in vivo* approach to test the pseudo-phosphorylation mediated rescue of HCM phenotype in mice [19]. Echocardiography and invasive hemodynamic studies showed significant improvements of intact heart function in S15D-D166V mice compared with D166V, along with a rescue of largely reduced maximal tension and abnormally high myofilament Ca^{2+} sensitivity observed in D166V-mutated hearts [19]. These collective results formed the scientific basis for the present study, aimed to recover/mitigate the pathological D166V-induced abnormalities via adeno-associated virus (AAV) delivery of the S15D-RLC phosphomimic construct in the hearts of adult HCM-D166V mice.

Adeno-associated viral (AAV) vectors provide for safe, long-term gene transfer in a wide variety of animal organs, including skeletal muscle, liver and heart [24]. Various AAV serotypes exhibit natural tissue tropism, based on viral capsids recognizing specific viral receptors expressed on specific cell types that can be exploited to enhance gene delivery to one specific organ over another. Serotypes AAV6, AAV8 and AAV9 have been shown to transduce cardiomyocytes preferentially following systemic administration and provide uniform gene delivery throughout the cardiac muscle [25, 26]. We have constructed AAV9 vectors where the cytomegalovirus (CMV) promoter drives the expression of the S15D-RLC phosphomimic construct with an IRES-dependent expression of human recombinant green fluorescent protein (hrGFP) reporter gene. The data show that the AAV9-based expression of S15D-RLC in D166V mice improves intact cardiac function as assessed via echocardiography, invasive hemodynamics and muscle mechanics study compared to PBS-injected D166V counterparts. To our understanding, this is the first *in vivo* study that has explored AAV9-S15D-RLC gene therapy in the treatment/mitigation of HCM phenotype in mice caused by a malignant RLC mutation.

Materials and Methods

Transgenic HCM-D166V mouse model

All animal procedures and experiments were performed in accordance with the "Guide for the Care and Use of Laboratory Animals" (NIH). UM has an Animal Welfare Assurance on file with the Office of Laboratory Animal Welfare (OLAW), NIH. The assurance number is #A-3224-01, effective November 24, 2015. IACUC protocol # is 18-110. Mice were euthanized through CO_2 inhalation followed by cervical dislocation.

Transgenic humanized WT-RLC and D166V mice used in this study were generated previously [13]. The founder mice have been bred to non-transgenic (NTg) B6SJL mice. Female (F) and male (M) mice were used in AAV-based gene therapy. D166V mice were 5.5±1 and 7±1 months of age and WT were 6±0.5 and 5.5±0.5 month-old at the time of AAV-S15D-RLC and PBS injections, respectively. All injected mice were evaluated for improvements of heart function ~1 month post-injection.

Plasmid generation and AAV virus production

A plasmid in which the cytomegalovirus (CMV) promoter drives the expression of the human ventricular RLC carrying the Ser-15 to Aspartic acid mutation was used to generate rAAV9-pseudotyped viral particles. AAV9-based vector genomes were cross-packaged into AAV9 capsids via the triple transfection of HEK 293T cells, then purified by iodixanol gradient centrifugation and FPLC purification. Titers of the AAV vectors (viral genomes/ml) were determined by quantitative real-time PCR. The following primers were used for amplifying human growth hormone (hGH) PolyA: 5′-CTATTGGGAACCAAGCTGGA-3′ (forward) and 5′-GTGAAACCCCGTCTCTACCA-3′ (reverse). The plasmid used as standard was the pAAV-eGFP-WPRE, which was packed for empty AAV virus, also harboring CMV-driven eGFP followed by woodchuck hepatitis virus posttranscriptional regulatory element.

AAV9-S15D-RLC delivery in D166V HCM and WT-RLC mice

Mice were anesthetized by inhalation with 1-3% isoflurane and body temperatures were maintained at 37°C during the entire procedure. When the mice were unresponsive to toe-pinch, the left side of the chest was coated with depilatory (Veet) to remove fur from the skin. Each limb was immobilized using tape. A sterile 30-gauge needle attached to a 100μl Hamilton syringe (or regular insulin sterile syringe for thoracic cavity), preloaded with the injectate was used to slowly advance through the skin, intercoastal and into the myocardial chamber/pleural space in the case of thoracic cavity injection. Depending on the difficulty of piercing the needle through the skin, the needle was slightly inclined with respect to the vertical direction to the skin surface. For direct LV cavity injections, the syringe plunger was pulled to confirm that the blood is drawn from the left ventricle chamber to ensure systemic delivery. A total of 50 μl (100 μl for thoracic) of the injectate (either PBS control or 1.4×10^{11} vg diluted in sterile PBS) was delivered per mouse. The needle was then removed. Any bleeding was stopped by gently application of a cotton-tipped applicator onto the needle insertion site. The isoflurane system was turned off. Once rhythmic, rapid, shallow breathing was verified, and the animal started moving, the mouse was returned to its cage.

Characterization of AAV-injected heart tissue by PCR, fluorescence microscopy and 2D SDS-PAGE

DNA was extracted from flash-frozen heart tissue using the Accustart II mouse genotyping kit (Quanta Biosciences). The S15D-RLC-IRES-hrGFP vector genome were amplified with a forward primer corresponding to the beta globin intron and a reverse primer corresponding to the human RLC. Mouse actin gene was used as an internal control. GFP fluorescence images were taken by Olympus IX-81, an advanced motorized inverted fluorescence microscope system with 10, 20 and 40× objectives and an F-view cooled CCD camera, utilizing Cell-R Live Imaging software for data acquisition and analysis. Exposure time for AAV-S15D-RLC-GFP/AAV-empty injected samples varied from 6.7-9.4 ms, while that for non-injected samples was 210 ms. Intrinsic GFP fluorescence was assessed in freshly dissected heart tissue washed with ice cold PBS.

The incorporation of S15D-RLC protein in mouse myocardium (myosin) was documented by two-dimensional (2D) SDS-PAGE of AAV-9 vs. PBS -injected mice. Performing 2D-electrophoresis was a necessity due to the lack of MW (molecular weight) difference between ventricular isoforms of human (AAV-injected) vs. mouse (endogenous) RLCs that are characterized by different pI values (pI=4.98 for D166V and pI=4.82 for S15D-RLC) allowing for their clear separation via isoelectric focusing. For 2D-PAGE, myosin purified from left ventricles of mouse hearts, prepared as described previously [27], were further processed using 2D Clean-up kit (to remove interfering substances such as salts, lipids, nucleic acids and detergents) and then resuspended in IEF buffer containing 8M urea, 2% CHAPS, 0.5% carrier ampholyte, 40 mM DTT and 0.002% Bromophenol blue. Samples were loaded into Immobiline DryStrip gels (IPG strips, pH 4-7) and first dimension - isoelectric focusing was performed followed by the 2nd dimension – SDS-PAGE. Presence of S15D-RLC protein was visualized by Western blotting using CT-1 antibody, produced in this lab [28] that recognizes the total RLC protein, followed by a goat anti-rabbit antibody conjugated with the fluorescent dye, IR red 800. Myosin ELC, detected with ab680 antibody (Abcam) was used as a loading control [19, 29]. Bands intensities were quantified using ImageJ (imagej.nih.gov/ij).

Echocardiography and invasive hemodynamics (P-V loops) experiments

Conventional Echocardiography: *In vivo* cardiac morphology and function studies were performed as described previously [19, 27, 29]. A Vevo-2100 imaging system, equipped with MS400 transducer, was used for echocardiography evaluations. Mice were anesthetized by inhalation with 1-3% isoflurane and body temperatures were maintained at 37°C. B-mode and M-mode images were saved for analysis using Vevo Lab 1.7.1 software (Visual Sonics Inc.). End-diastolic and end-systolic endocardial volumes were calculated from bi-dimensional long-axis parasternal views [19]. Left ventricular diastolic function was analyzed using the values derived from mitral flow inflow velocity curves obtained by pulsed Doppler mode.

Tei Index: Global cardiac dysfunction was assessed by measuring Myocardial Performance Index (MPETei index), originally described by Tei and his colleagues [30]. MPI was calculated using the following equation:

$$\text{LV MPI} = \frac{\text{IVCT+IVRT}}{\text{ET}} = \frac{X - Y}{Y}$$

where X describes the interval from the cessation to onset of transmitral inflow and is equal to the sum of isovolumic contraction time (IVCT), ejection time (ET), and isovolumic relaxation time (IVRT), and Y describes the ejection time (ET).

Speckle Tracking-Based Echocardiographic (STE) Strain Analysis: High resolution long-axis B-mode images (digitally stored as 300 frames cine loops) were used to perform STE analyses using the Vevo strain software (Vevo LAB 2.1.0). Strain, which assesses change in length relative to initial length (Strain = final length [l]/initial length [lo]) and Strain rate (SR), which describes the rate of change of deformation over time (Strain rate=strain/time) were measured in the radial axis (from the center of the ventricular cavity outward) and in the longitudinal axis (from the apex to the base). Furthermore, Global and regional (six segments: anterior basal/mid/apical and posterior basal/mid/apical) LV longitudinal and radial strain (in peak strain %) and strain rates were evaluated in both epicardial and endocardial regions. In addition, B-mode images were recorded, with vector diagrams depicting magnitude and direction of endocardial deformation. Left ventricular global longitudinal strain (GLS) measurements of the maximal shortening of myocardial longitudinal length during systole were compared to the resting length in diastole. Greater degrees of deformation are expressed as a numerically lower (more negative) strain values. Conventional echo parameters such as Cardiac output (CO_{str}). Ejection fraction (EF_{str}), Fractional shortening (FS_{str}), Stroke volume (SV_{str}), End Diastolic Volume (EDV_{str}) were also calculated from strain analysis.

Invasive Hemodynamics Evaluation: Mice were anesthetized by intubation with 1-2% isoflurane and body temperature was maintained at 37°C. A 6% albumin solution was infused into the jugular vein at the rate of 5 μl/min. A catheter (SPR-839; Millar Instrument, Houston, TX) transducer was introduced into the left ventricle through the right carotid artery. The pressure-volume (P-V) loops were recorded at steady state and during the inferior vena cava (IVC) occlusions [19, 27, 29].

Skinned cardiac papillary muscle fibers and assessment of contractile force

Left ventricular (LV) papillary muscles from AAV vs PBS vs empty vector injected mice were isolated and dissected into muscle bundles in the buffer containing pCa 8 solution (10^{-8}M [Ca^{2+}], 1 mM free [Mg^{2+}] (total MgPr (propionate) =3.88 mM), 7 mM EGTA, 2.5 mM [Mg-$ATP^{2'}$), 20 mM MOPS, pH 7.0, 15 mM creatine phosphate, and 15 units/mL phosphocreatine kinase, ionic strength =150 mM adjusted with KPr), 15% (vol/vol) glycerol, and 30 mM BDM. The papillary muscle bundles were then skinned in 50% pCa 8 solution and 50% glycerol containing 1% (vol/vol) Triton X-100 for 24 h at 4 °C, and then they were then transferred into the same solution without Triton X-100 and stored at −20 °C until used [19, 27]. On the day of experiment, muscle strips (~1.4 mm in length and 100 μm in diameter) were isolated from glycerinated skinned mouse papillary muscle bundles and attached to a Guth force transducer. The sarcomere length was adjusted to ~2.1 μm, and the

maximal steady state force at pCa 4 (expressed in kN/m^2) and the force-pCa dependence were established for all experimental and control mice [19, 27].

Assessment of fibrosis

The hydroxyproline (HOP) content in the hearts of mice was measured by hydroxyproline (HOP) assay as described previously [27, 29]. Briefly, 15-22 mg of flash frozen LV heart tissue were isolated from 7-8 D166V and 3-6 WT mice and boiled in 200 μL of 6 M HC1 at 110°C overnight. Five-μL aliquots of hydrolyzed tissue were added to 80 μL of 100% isopropanol and allowed to react with 40 μL of 7% chloramine-T solution mixed at a 1:4 ratio with acetate citrate buffer for 5 min at room temperature. Then, 0.5 mL Ehrlich reagent was added to the mixture at a 3:13 ratio with isopropanol and incubated at 55 °C for 30 min. Then the mixture was placed on ice for 5 min and centrifuged at 5,000 × g for 1 min at 4°C. 200 μL aliquots were placed in a 96-well plate and the absorbance was measured at 558 nm. The standard curve of trans-4-hydroxy-L-proline (0 to 1,000 μM) was used to determine the total amount of HOP in ventricles (in mg) of all tested mice. Assay was performed in triplicate on n= 5-13 heart samples from D166V and WT animals.

Statistical analyses

All values are shown as means ± SEM (standard error of the mean). Statistically significant differences between two groups were determined using an unpaired Student's *t*-test and comparisons between multiple groups were performed using one-way or two-way ANOVA for independent variable or multiple factors, respectively, followed by Tukey's multiple comparison test (GraphPad Prism 7). Significance was defined as *P<0.05, **P<0.01, and ***P<0.001 and ****p<0.0001.

Standard sample sizes were chosen for all experiments. Exact sample sizes for experiments are shown in figures and table. Statistical methods were not used for predetermination of power. All animals were randomly allocated to AAV and control groups and were handled equally. Operators who performed AAV/control injections and functional analyses were blinded to group identity. No data points were excluded.

Results

Characterization of AAV virus

Figure 1A shows the schematic of the plasmid vector used for the production of recombinant AAV particles (top panel). The S15D-RLC construct containing the Serine-to-Aspartic acid (S15D) substitution, was cloned into ITR/MSC-containing pAAV-IRES-hrGFP. The vector also contains a dicistronic expression cassette, expressing the humanized recombinant green fluorescent protein (hrGFP), as a second open reading frame that is translated from the encephalomyocarditis virus (EMCV) internal ribosome entry site (IRES). Bottom panel in Figure 1A represents fluorescence microscopy images of cultured HEK293T cells transfected with the recombinant plasmid vector. 69μg of the plasmid vector was used to transfect 293 T cells that were seeded at a density of 80 million per flask (875cm^2). The strategy for AAV9-S15D-RLC delivery and assessment of heart function is presented in Figure 1B. AAV9 virus particles were injected via direct LV cavity injection in the hearts of

D166V and WT mice at 1.4×10^{11} vg per mouse. The therapeutic effect of the phosphomimic S15D-RLC molecule was tested *in vivo* by echocardiography (conventional as well as by speckle-based strain analysis) and PV-loops. All mice were examined in a blinded fashion prior to the AAV vs. PBS injections by echocardiography, and then 1 month post-injection by echocardiography and invasive hemodynamics. Then, the mice were sacrificed, and papillary muscles were isolated and evaluated for the ability of myosin to interact with actin and develop contractile force while the cardiac tissues were used for AAV characterization. Strong GFP fluorescence within the cardiomyocytes was observed in AAV-injected D166V HCM mice compared to non-injected/empty vector injected D166V control mice (Figure 2). The presence of AAV virus was detected in ventricular tissue of AAV-injected non-transgenic mice (Figure 3A, **left panel**) well as in transgenic D166V mice (Figure 3A, **right panel**) by PCR. The incorporation of S15D-RLC in the cardiac myosin of D166V mice was also documented by 2D SDS-PAGE/Westem blotting, using the CT-1 antibody specific for the RLC (Figure 3B). Myosin essential light chain (ELC) was used as a loading control. As shown in Figure 3B, average S15D-RLC expression in left ventricles of AAV9-injected D166V mice (n=7 samples from 5 animals) was 31±5% (mean ±SD, standard deviation). Average D166V RLC expression in non-injected mice was 93±6% (n=7 samples from 2 animals) and in S15D-RLC injected D166V mice, it was 76±14 (n=10 samples from 6 animals). Achieved levels of S15D-RLC incorporation in the myocardium of mice are well within physiological levels of RLC phosphorylation in the healthy heart [31], and thus sufficient to achieve a therapeutic effect.

Assessment of heart function in AAV- vs PBS- injected HCM-D166V mice by echocardiography and invasive hemodynamics

Assessment of cardiac morphology and function in AAV9-injected vs PBS injected D166V and WT mice was assessed via echocardiography and invasive pressure-volume loops and are presented in Figure 4 and Table 1. Measurements of heart function were also performed for control AAV vs PBS injected WT-RLC mice. The average heart rate was 490±14 and 504±31 for AAV- and PBS-injected D166V, respectively and 452±20 and 424±30 for AAV- and PBS-injected WT, respectively. Echocardiography measurements revealed a significant recovery in hypertrophic chamber dimensions such as decrease in the left ventricular anterior wall (LVAW) thickness in diastole (Figure 4A) and in left ventricular posterior wall (LVPW) thickness in systole and diastole (Table 1). Consistently, a significant increase in LV inner diameter in diastole and in LV diastolic volume were observed in AAV-injected D166V mice compared to PBS controls. These results suggest an AAV-mediated successful mitigation of hypertrophic morphology of HCM-D166V hearts.

Similarly, invasive hemodynamics data showed an increase in cardiac output (CO) in AAV-injected D166V mice, suggesting increased pumping ability of the heart (Figure 4A). Similarly, the peak rate of rise in LV pressureμvolume relationship (dP/dtmax-EDV) was observed to be significantly lower in PBS-injected D166V, indicating a compromised ionotropic cardiac function in PBS-treated hearts, which was significantly improved in AAV-injected D166V animals. Likewise, a largely reduced preload recruitable power stroke work (PRSW) was normalized in AAV vs PBS controls. Phosphomimic delivery also led to a decrease in isovolumic relaxation constant Tau (in milliseconds), which was observed to be

prolonged in HCM-D166V mice (Figure 4A). Interestingly, the PBS-injected hearts showed similar characteristics to sedentary D166V mice published previously [19] while S15D-RLC injected animals bear similarities to transgenic double S15D-D166V mice [19]. Figure 4B depicts measurements of heart function in AAV vs PBS injected WT animals. With the exception of dP/dtmax-EDV, the AAV treatment did not produce any changes in heart function compared with PBS-treated WT mice, suggesting that the AAV9-S15D-RLC therapy works to alleviate the consequences of HCM disease and does not change the function of normally working WT-RLC hearts (Figure 4B).

Figure 4C characterizes myocardial performance (MPI) in AAV- vs PBS-injected D166V and WT mice by strain analysis. Consistent with data in Figure 4A, AAV-treated D166V mice showed significantly lower MPI index compared to PBS-injected animals, while no changes were observed in WT mice (Figure 4C). The data are indicative of better global cardiac function in AAV-treated D166V but not in AAV-treated WT mice. Strain analysis of B-mode images further validated successful AAV-therapy and mitigating the consequences of HCM in D166V mice, while WT hearts remained unaffected by AAV treatment (Figure 5). As shown in Figure 5A, AAV-mediated improvements in D166V mice were observed in cardiac output (CO_{str}), End-diastolic Volume (EDV_{st}), Ejection fraction (EF_{str}), Fractional shortening (FS_{str}), and Stroke Volume (SV_{str}) (Table 1). Similarly, GLS (global longitudinal strain) analysis showed enhanced myocardial shortening in AAV vs PBS-injected D166V mice, manifested by significantly lower (more negative) values, indicating enhanced deformation/shortening. Figure 5B shows representative three-dimensional LV longitudinal strain deformation diagrams from D166V (top panels) and WT (bottom panels) for AAV (left panels) vs PBS (right panels) animals. The deformation shows contraction (red/positive values) or relaxation (blue/negative values) over six LV segments during four consecutive cardiac cycles. Note that LV longitudinal strain deformation has a different scale for AAV- and PBS-injected mice, as preset by the Vevo Software, and hence, to facilitate images' interpretation/comparison of two groups, an orange line linked the scales of two graphs (Figure 5B).

Improvement of contractile function in skinned papillary muscle strips from AAV-S15D-RLC treated HCM mice

Assessment of maximal force development and calcium sensitivity of force in skinned papillary muscle fibers from AAV9-S15D-RLC injected D166V and WT mice vs controls was achieved in papillary muscle strips (~1.4 mm in length and 100 μm in diameter) that were isolated from glycerinated muscle bundles and attached to a Guth force transducer. In addition to PBS-injected and non-injected animals, the control group included animals injected with an empty AAV-vector (three mice per group). One empty vector injected heart yielded about 5 good quality muscle fibers providing enough data points (n=15) to fully assess contractile mechanics in this control group of mice (Figure 6). A significant recovery in maximal isometric force (in $kN/m^2 \pm SD$) in AAV-injected D166V mice (44.8±5.1) compared to either PBS (31.7±5.2), empty (35.9±0.6) or non-injected (30.0±3.1) mice was observed (Figure 6A). Compared to D166V, WT fibers demonstrated significantly higher maximal tension across all groups: AAV (53.8±0.5), PBS (54.8±0.6), empty (55.3±2.0) and non-injected (54.0±0.5) animals; however, there was no effect on AAV vs control treatments

in WT mice (Figure 6B). As shown previously [19], non-injected D166V HCM mice showed significantly increased calcium sensitivity of force, pCa_{50} (5.81±0.08) compared to non-injected WT (5.65±0.09). However, no significant changes were seen in pCa_{50} upon AAV (5.83±0.05), PBS (5.76±0.05) or empty (5.77±0.01) treatment for D166V or WT: AAV (5.71±0.01), PBS (5.68±0.01), empty (5.68±0.02) or non-injected (5.65±0.09) animals (Figure 6).

Assessment of fibrosis by hydroxyproline (HOP) assay

Quantification of fibrosis in the hearts of AAV9-S15D-RLC injected D166V and WT mice compared with PBS/non-injected controls is presented in Figure 7. The HOP content was measured in female and male mice (n=5-13 heart samples from 7-8 D166V and 3-6 WT animals) as described previously [29]. As expected PBS injected D166V mice showed a higher HOP content compared to PBS injected WT mice. Importantly, there was a significant difference between PBS and AAV injected HCM-D166V mice ($P<0.05$), suggesting that the treatment with AAV9-S15D-RLC may be beneficial in alleviating HCM-mediated fibrosis (Figure 7).

Discussion

Since the discovery of the existence of myosin light chains as charged variants by Perry's group [32], RLC phosphorylation has emerged as an indispensable modulator of striated muscle contraction. Reports have shown enhanced force generation induced by RLC phosphorylation, and HCM-causing RLC mutations have been associated with depressed endogenous levels of myosin RLC phosphorylation [13, 14, 19]. This study focuses on D166V RLC variant shown to cause HCM in humans and in D166V mice, and these pathological changes observed in mouse hearts coincide with low levels of RLC phosphorylation *in situ* [13]. Using recombinant pseudo-phosphorylated RLC proteins, we demonstrated that the S15D phosphomimic was able to abrogate the majority of the detrimental effects induced by the D166V mutation *in vitro* [23]. However, with exception of our transgenic S15D-D166V rescue mice [19], no previous study has assessed the efficacy of this targeted approach *ex vivo* in the context of the heart carrying a disease-causing HCM mutation. In this report, by delivering S15D-RLC via a cardiotropic adeno-associated virus serotype 9 (AAV9) and characterizing physiologically and therapeutically relevant amount of phosphomimic protein expression in the mutant mice myocardium, we have shown a marked improvement in intact cardiac morphology as well as function *in vivo*, along with an increase in maximal force generation capability in papillary muscles compared with controls.

Our two decade-long research on myosin regulatory light chains continues providing insight into HCM-mutation specific impact on myosin motor function and the contractile properties of papillary muscle fibers from the hearts of mouse models of RLC-related HCM. Importantly, we observe a correlation between the severity of HCM phenotype and the level of cardiac RLC phosphorylation *in situ* in mice [13, 14, 19]. The D166V mutation, reported to be associated with malignant HCM phenotype in humans [21], largely impacted myosin RLC phosphorylation in the hearts of mice as tested in rapidly frozen ventricular samples

from D166V mice, and in skinned papillary muscle fibers from animal hearts used for determination of actin-myosin interaction and force development [13, 19, 22]. Concurrently with a reduced level of endogenous RLC phosphorylation, we observed a decompensated contractile function in HCM animals preventing the diseased hearts from efficiently pumping blood [13, 14, 19, 33]. In support of animal studies, low levels of RLC phosphorylation are also observed in clinical studies on HF patients [11, 12, 34]. The mechanistic basis for this phenomenon is likely the decreased ability of dephosphorylated myosin to efficiently execute the power stroke and generate enough force to maintain normal heart function compared with myosin whose RLCs maintain the physiological levels of myosin phosphorylation, i.e. ~0.4 mole Pi/mole RLC [31, 35]. Unraveling the molecular basis of RLC-mutant mediated cardiac dysfunction opened new possibilities for effective treatments and suggested RLC phosphorylation as a target for novel heart therapy in HCM.

In this study, we aimed to test a new method to reverse the effects of HCM, caused by the D166V mutation, using a highly effective strategy of AAV-mediated gene delivery. The proof-of-principle was recently published [19, 36], where we showed that the functional, structural and histological phenotypes observed in HCM-D166V mice could be prevented by cardiac-specific expression of phosphomimic S15D-D166V. Importantly, experiments in S15D-D166V mice demonstrated that the depressed RLC phosphorylation in D166V myocardium was not a product of reduced cMLCK expression, and that the hypo-phosphorylation of myosin RLC in D166V hearts was most likely a result of mutation-elicited steric constraints preventing cMLCK to effectively phosphorylate RLC at Ser15 [19, 22]. The current study was designed to test this hypothesis and restore a unique structural/charge balance by introducing the S15D phosphomimic RLC via a highly robust AAV9 expression system shown by many to last for approximately 1 year [24–26, 37]. The AAV9 virus was conjugated with the CMV promoter to efficiently express S15D-RLC in the hearts of mice. The ~30% of S15D-RLC incorporation appears to match the physiological levels of myosin phosphorylation, i.e. ~0.4 mole Pi/mole RLC required for the normal function of the heart [31, 35].

Significant improvements in heart performance as well as an increased contractile function were noted in AAV-treated D166V animals compared with control groups of mice while no changes were seen between AAV vs PBS injected WT-RLC mice. Tei index (or MPI) that incorporates both systolic and diastolic time intervals in expressing global systolic and diastolic ventricular function was found to be significantly increased in PBS vs AAV injected D166V animals, but was unchanged in WT mice. The Tei-Index has been shown to serve as a sensitive indicator of overall cardiac dysfunction in patients with mild-to-moderate congestive heart failure [38]. Consistent with these assessments, global longitudinal strain analysis which showed impaired heart function in PBS-injected D166V animals revealed a significant improvement in AAV-treated D166V hearts marked by increased myocardial shortening and suggesting enhanced contractility. Interestingly, there was a significant difference in HOP content between PBS and AAV injected HCM-D166V mice, suggesting that the treatment with AAV9-S15D-RLC may be beneficial in alleviating HCM-mediated fibrosis.

The results with AAV9-S15D-RLC injected WT mice revealed that the addition of phosphomimic RLC variant to WT myocardium does not change its function, and this lack of effect is most likely due to the ability of WT-RLC to become phosphorylated with endogenous cMLCK in WT hearts. This is in contrast to D166V mice showing no to very little RLC phosphorylation despite normal levels of cMLCK expression [19]. We hypothesize that the D166V-elicited inhibitory conformation at the RLC Ser-15 phosphorylation site prevents the cMLCK to efficiently phosphorylate cardiac myosin motors and their low level of phosphorylation leads to decompensated cardiac function. We further hypothesize that the phosphorylatable RLC in WT myocardium works well without additional S15D molecular trigger that is required to release the inhibitory RLC conformation in HCM hearts. In summary, we showed here that the AAV9-S15D therapy works to alleviate the consequences of HCM disease and does not change the function of normally working WT-RLC hearts.

Limitations and future approaches:

A methodological limitation of our study is the sample size that will need to be increased for more power. To increase robustness and fidelity of our approach, future *in vivo* studies are needed on transgenic WT-RLC and D166V-HCM animals that in addition to AAV9-S15D-RLC vs PBS treatments will be injected with AAV9-WT-RLC and AAV9-empty vectors. This is to definitively conclude whether the AAV-S15D-RLC mediated improvement of heart function observed in AAV vs PBS treated HCM mice, which is observed here, is specific to the S15D-delivery and do not arise from a decreased expression of an HCM-RLC gene replaced with S15D-RLC in AAV-treated HCM mice. In addition, structural studies are needed to elaborate on the molecular mechanisms by which D166V HCM mutation might confer inhibitory RLC-Ser15 conformation and to interrogate the structural effects of S15D phosphomimic constructs.

Concluding remarks:

Genetic cardiomyopathies are the most prevalent inherited heart diseases and no therapies are currently available to cure or delay progression from hypertrophy to HF, and/or to prevent SCD. Notably, familial HCM is the most frequently occurring inherited cardiac disease that is considered to be the leading cause of SCD in otherwise healthy young athletes. It is not possible to revert HCM-causing mutations back to their wild-type state and it is therefore critical to elucidate the mechanism of the disease and identify gene/protein-specific therapeutic targets that could lessen disease progression and improve quality of life. Our combined data demonstrate that RLC pseudo-phosphorylation is able to enhance actomyosin function and heart performance, and that targeting RLC phosphorylation may be an important element in clinical management of HCM. The *in vivo* and *in vitro* metrics of improved myocardial function in HCM-D166V animals provide a solid platform for future experiments to further explore myosin regulatory light chain biology as a potential tool in clinical setting to treat RLC-related HCM. To our understanding, this is the first study to characterize a robust *in vivo* AAV gene therapy using an RLC phosphomimic to mitigate the detrimental consequences and improve cardiac function in humanized mice models of HCM.

Acknowledgments:

This work was supported by the National Institutes of Health R01-HL123255 (DSC) and the American Heart Association: 17PRE33650085 (SY), 15PRE23020006 (CCY) and 12PRE12030412 (WH).

References

1. Ho CY (2010) Hypertrophic cardiomyopathy. Heart Fail Clin 6: 141–159. [PubMed: 20347784]
2. Alcalai R, Seidman JG, Seidman CE (2008) Genetic Basis of Hypertrophic Cardiomyopathy:From Bench to the Clinics. J Cardiovasc Electrophysiol 19: 104–110. [PubMed: 17916152]
3. Maron BJ (2002) Hypertrophic cardiomyopathy: a systematic review. JAMA 287: 1308–1320. [PubMed: 11886323]
4. Szczesna-Cordary D (2003) Regulatory light chains of striated muscle myosin. Structure,function and malfunction. Curr Drug Targets Cardiovasc Haematol Disord 3: 187–197. [PubMed: 12769642]
5. Alfares AA, Kelly MA, McDermott G, Funke BH, Lebo MS, Baxter SB, Shen J, McLaughlin HM, Clark EH, Babb LJ, et al. (2015) CORRIGENDUM: Results of clinical genetic testing of 2,912 probands with hypertrophic cardiomyopathy: expanded panels offer limited additional sensitivity. Genet Med 17: 319. [PubMed: 25835197]
6. Gaita F, Di Donna P, Olivotto I, Scaglione M, Ferrero I, Montefusco A, Caponi D, Conte MR, Nistri S, Cecchi F (2007) Usefulness and safety of transcatheter ablation of atrial fibrillation in patients with hypertrophic cardiomyopathy. Am J Cardiol 99: 1575–1581. [PubMed: 17531584]
7. Szczesna-Cordary D, Guzman G, Ng SS, Zhao J (2004) Familial hypertrophiccardiomyopathy-linked alterations in Ca^{2+} binding of human cardiac myosin regulatorylight chain affect cardiac muscle contraction. J Biol Chem 279: 3535–3542. [PubMed: 14594949]
8. Rayment I, Rypniewski WR, Schmidt-Base K, Smith R, Tomchick DR, Benning MM, Winkelmann DA, Wesenberg G, Holden HM (1993) Three-dimensional structure of myosin subfragment-1: a molecular motor. Science 261: 50–58. [PubMed: 8316857]
9. Szczesna D, Ghosh D, Li Q, Gomes AV, Guzman G, Arana C, Zhi G, Stull JT, Potter JD(2001) Familial hypertrophic cardiomyopathy mutations in the regulatory light chains of myosin affect their structure, Ca^{2+} binding, and phosphorylation. J Biol Chem 276: 7086–7092. [PubMed: 11102452]
10. Yadav S, Szczesna-Cordary D (2017) Pseudophosphorylation of cardiac myosin regulatorylight chain: a promising new tool for treatment of cardiomyopathy. Biophys Rev 9: 57–64. [PubMed: 28510043]
11. van der Velden J, Papp Z, Boontje NM, Zaremba R, de Jong JW, Janssen PM, Hasenfuss G, Stienen GJ (2003) Myosin light chain composition in non-failing donor and end-stage failing human ventricular myocardium. Adv Exp Med Biol 538: 3–15. [PubMed: 15098650]
12. van der Velden J, Papp Z, Boontje NM, Zaremba R, de Jong JW, Janssen PML, Hasenfuss G, Stienen GJM (2003) The effect of myosin light chain 2 dephosphorylation on Ca^{2+}-sensitivity of force is enhanced in failing human hearts. Cardiovasc Res 57: 505–514. [PubMed: 12566123]
13. Kerrick WGL, Kazmierczak K, Xu Y, Wang Y, Szczesna-Cordary D (2009) Malignantfamilial hypertrophic cardiomyopathy D166V mutation in the ventricular myosin regulatory light chain causes profound effects in skinned and intact papillary muscle fibers from transgenic mice. FASEB J 23: 855–865. [PubMed: 18987303]
14. Abraham TP, Jones M, Kazmierczak K, Liang H-Y, Pinheiro AC, Wagg CS, Lopaschuk GD, Szczesna-Cordary D (2009) Diastolic dysfunction in familial hypertrophic cardiomyopathy transgenic model mice. Cardiovasc Res 82: 84–92. [PubMed: 19150977]
15. Scruggs SB, Hinken AC, Thawornkaiwong A, Robbins J, Walker LA, de Tombe PP, Geenen DL, Buttrick PM, Solaro RJ (2009) Ablation of ventricular myosin regulatory light chain phosphorylation in mice causes cardiac dysfunction in situ and affects neighboring myofilament protein phosphorylation. J Biol Chem 284: 5097–5106. [PubMed: 19106098]
16. Sheikh F, Ouyang K, Campbell SG, Lyon RC, Chuang J, Fitzsimons D, Tangney J, Hidalgo CG, Chung CS, Cheng H, et al. (2012) Mouse and computational models link Mlc2v dephosphorylation to altered myosin kinetics in early cardiac disease. J Clin Invest 122: 1209–1221. [PubMed: 22426213]

17. Huang J, Shelton JM, Richardson JA, Kamm KE, Stull JT (2008) Myosin regulatory lightchain phosphorylation attenuates cardiac hypertrophy. J Biol Chem 283: 19748–19756. [PubMed: 18474588]

18. Warren SA, Briggs LE, Zeng H, Chuang J, Chang EI, Terada R, Li M, Swanson MS, Lecker SH, Willis MS, et al. (2012) Myosin light chain phosphorylation is critical for adaptation to cardiac stress. Circulation 126: 2575–2588. [PubMed: 23095280]

19. Yuan CC, Muthu P, Kazmierczak K, Liang J, Huang W, Irving TC, Kanashiro-Takeuchi RM, Hare JM, Szczesna-Cordary D (2015) Constitutive phosphorylation of cardiac myosin regulatory light chain prevents development of hypertrophic cardiomyopathy in mice. Proc Natl Acad Sci U S A 112: E4138–4146. [PubMed: 26124132]

20. Muthu P, Huang W, Kazmierczak K, Szczesna-Cordary D (2012) Functional Consequencesof Mutations in the Myosin Regulatory Light Chain Associated with Hypertrophic Cardiomyopathy In: Veselka J (Ed) Cardiomyopathies – From Basic Research to Clinical Management. Ch. 17. InTech, Croatia: pp 383–408.

21. Richard P, Charron P, Carrier L, Ledeuil C, Cheav T, Pichereau C, Benaiche A, Isnard R, Dubourg O, Burban M, et al. (2003) Hypertrophic cardiomyopathy: Distribution of disease genes, spectrum of mutations, and implications for a molecular diagnosis strategy. Circulation 107: 2227–2232, and erratum (2004), 2109(2225), p.3258 [PubMed: 12707239]

22. Muthu P, Kazmierczak K, Jones M, Szczesna-Cordary D (2012) The effect of myosin RLCphosphorylation in normal and cardiomyopathic mouse hearts. J Cell Mol Med 16: 911–919 [PubMed: 21696541]

23. Muthu P, Liang J, Schmidt W, Moore JR, Szczesna-Cordary D (2014) In Vitro Rescue Studyof a Malignant Familial Hypertrophic Cardiomyopathy Phenotype by Pseudo-Phosphorylation of Myosin Regulatory Light Chain. Arch Biochem Biophys 552-553: 29–39. [PubMed: 24374283]

24. Bish LT, Morine K, Sleeper MM, Sanmiguel J, Wu D, Gao G, Wilson JM, Sweeney HL(2008) Adeno-associated virus (AAV) serotype 9 provides global cardiac gene transfer superior to AAV1, AAV6, AAV7, and AAV8 in the mouse and rat. Hum Gene Ther 19: 1359–1368. [PubMed: 18795839]

25. Konkalmatt PR, Wang F, Piras BA, Xu Y, O'Connor DM, Beyers RJ, Epstein FH, Annex BH, Hossack JA, French BA (2012) Adeno-associated virus serotype 9 administered systemically after reperfusion preferentially targets cardiomyocytes in the infarct border zone with pharmacodynamics suitable for the attenuation of left ventricular remodeling. J Gene Med 14: 609–620. [PubMed: 23065925]

26. Palomeque J, Chemaly ER, Colosi P, Wellman JA, Zhou S, Del Monte F, Hajjar RJ (2007)Efficiency of eight different AAV serotypes in transducing rat myocardium in vivo. Gene Ther 14: 989–997. [PubMed: 17251988]

27. Yuan CC, Kazmierczak K, Liang J, Zhou Z, Yadav S, Gomes AV, Irving TC, Szczesna-Cordary D (2018) Sarcomeric perturbations of myosin motors lead to dilated cardiomyopathy in genetically modified MYL2 mice. Proc Natl Acad Sci U S A 115: E2338–E2347. [PubMed: 29463717]

28. Wang Y, Xu Y, Kerrick WGL, Wang Y, Guzman G, Diaz-Perez Z, Szczesna-Cordary D(2006) Prolonged Ca^{2+} and force transients in myosin RLC transgenic mouse fibersexpressing malignant and benign FHC mutations. J Mol Biol 361: 286–299. [PubMed: 16837010]

29. Yuan CC, Kazmierczak K, Liang J, Kanashiro-Takeuchi R, Irving TC, Gomes AV, Wang Y, Burghardt TP, Szczesna-Cordary D (2017) Hypercontractile mutant of ventricular myosin essential light chain leads to disruption of sarcomeric structure and function and results in restrictive cardiomyopathy in mice. Cardiovasc Res 113: 1124–1136. [PubMed: 28371863]

30. Tei C, Ling LH, Hodge DO, Bailey KR, Oh JK, Rodeheffer RJ, Tajik AJ, Seward JB (1995)New index of combined systolic and diastolic myocardial performance: a simple and reproducible measure of cardiac function--a study in normals and dilated cardiomyopathy. J Cardiol 26: 357–366. [PubMed: 8558414]

31. Chang AN, Battiprolu PK, Cowley PM, Chen G, Gerard RD, Pinto JR, Hill JA, Baker AJ, Kamm KE, Stull JT (2015) Constitutive Phosphorylation of Cardiac Myosin Regulatory Light Chain in vivo. J Biol Chem.

32. Perrie WT, Smillie LB, Perry SB (1973) A phosphorylated light-chain component of myosinfrom skeletal muscle. Biochem J 135: 151–164. [PubMed: 4776866]

33. Huang W, Liang J, Kazmierczak K, Muthu P, Duggal D, Farman GP, Sorensen L, Pozios I, Abraham T, Moore JR, et al. (2014) Hypertrophic Cardiomyopathy Associated Lys104Glu Mutation in the Myosin Regulatory Light Chain Causes Diastolic Disturbance in Mice. J Mol Cell Cardiol 74: 318–329. [PubMed: 24992035]

34. van der Velden J, Papp Z, Zaremba R, Boontje NM, de Jong JW, Owen VJ, Burton PBJ, Goldmann P, Jaquet K, Stienen GJM (2003) Increased Ca^{2+}-sensitivity of the contractileapparatus in end-stage human heart failure results from altered phosphorylation of contractile proteins. Cardiovasc Res 57: 37–47. [PubMed: 12504812]

35. Chang AN, Mahajan P, Knapp S, Barton H, Sweeney HL, Kamm KE, Stull JT (2016)Cardiac myosin light chain is phosphorylated by Ca2+/calmodulin-dependent and - independent kinase activities. Proc Natl Acad Sci U S A 113: E3824–3833. [PubMed: 27325775]

36. Granzier HL, de Tombe PP (2015) Myosin light chain phosphorylation to the rescue. ProcNatl Acad Sci U S A 112: 9148–9149.

37. Prasad K-MR, Xu Y, Yang Z, Acton ST, French BA (2011) Robust Cardiomyocyte-SpecificGene Expression Following Systemic Injection of AAV: In Vivo Gene Delivery Follows a Poisson Distribution. Gene Therapy 18: 43–52. [PubMed: 20703310]

38. Bruch C, Schmermund A, Marin D, Katz M, Bartel T, Schaar J, Erbel R (2000) Tei-index inpatients with mild-to-moderate congestive heart failure. Eur Heart J 21: 1888–1895. [PubMed: 11052862]

Key messages

- HCM-D166V mice show decreased RLC phosphorylation and decompensated function
- AAV9-S15D-RLC gene therapy in HCM-D166V mice, but not in WT-RLC, results in improved heart performance
- Global longitudinal strain analysis shows enhanced contractility in AAV vs controls
- Increased systolic & diastolic function is paralleled by higher contractile force
- Phosphomimic S15D-RLC has a therapeutic potential for HCM

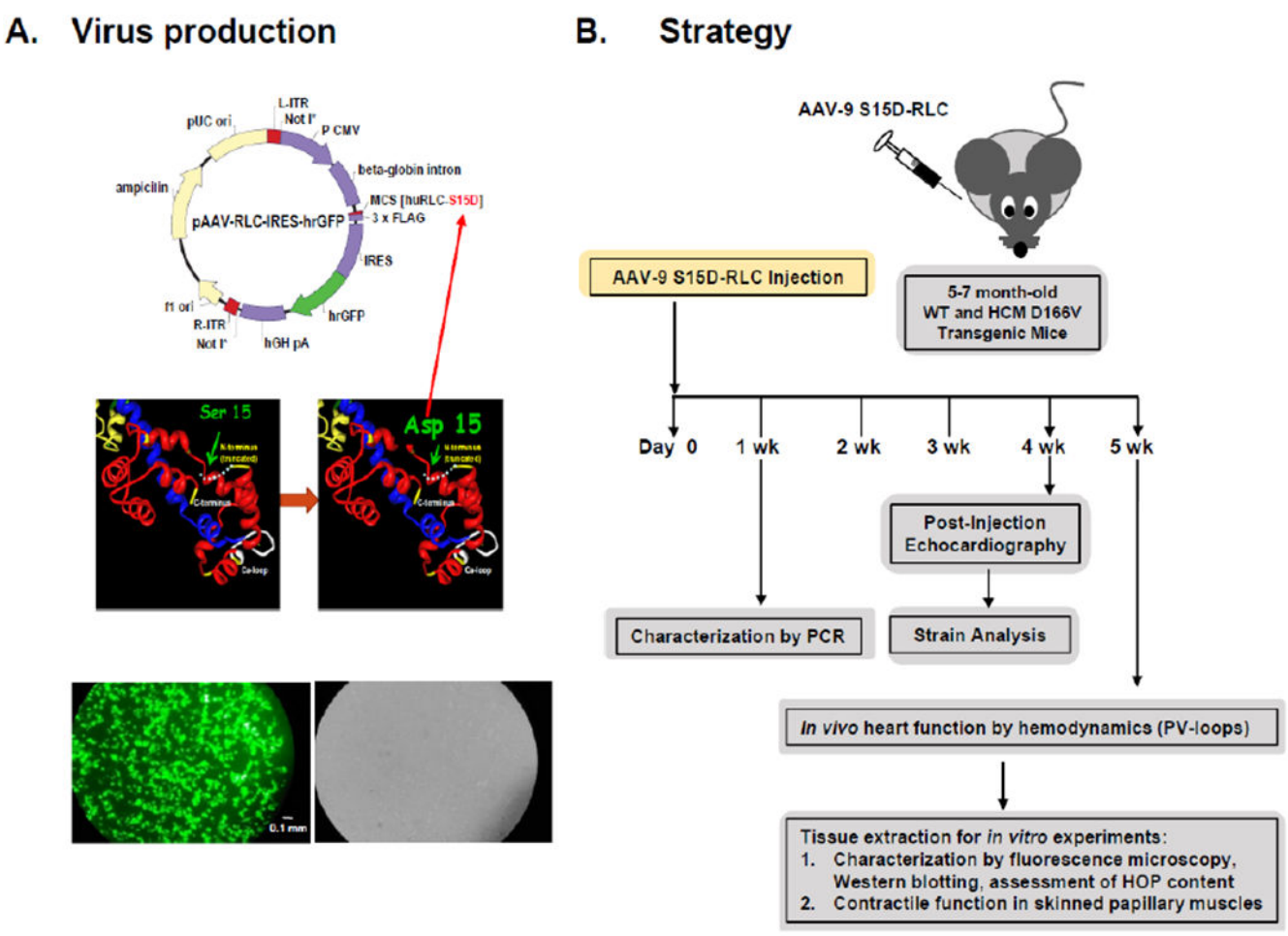

Figure 1.

A. Schematic representation of the AAV vector construct harboring the human cardiac S15D-RLC (huRLC-S15D-RLC) phosphomimic variant. Down panel: Fluorescence microscopy images of HEK293T cell culture transfected with pAAV-S15D-RLC-IRES-GFP (left-green fluorescence field; right-bright field). Scale bar is 0.1 mm. **B.** Overview of the AAV-gene therapy experiment: 5-7 mo-old WT and D166V HCM mice were injected with AAV9-S15D-RLC/PBS and were evaluated for the presence of virus via PCR and S15D-RLC protein via 2D-SDS-PAGE. 4-5 weeks post injection, the mice were evaluated for improvement of heart function by echocardiography (conventional and strain analysis), PV-loops, and contractile force measurement in skinned papillary muscles.

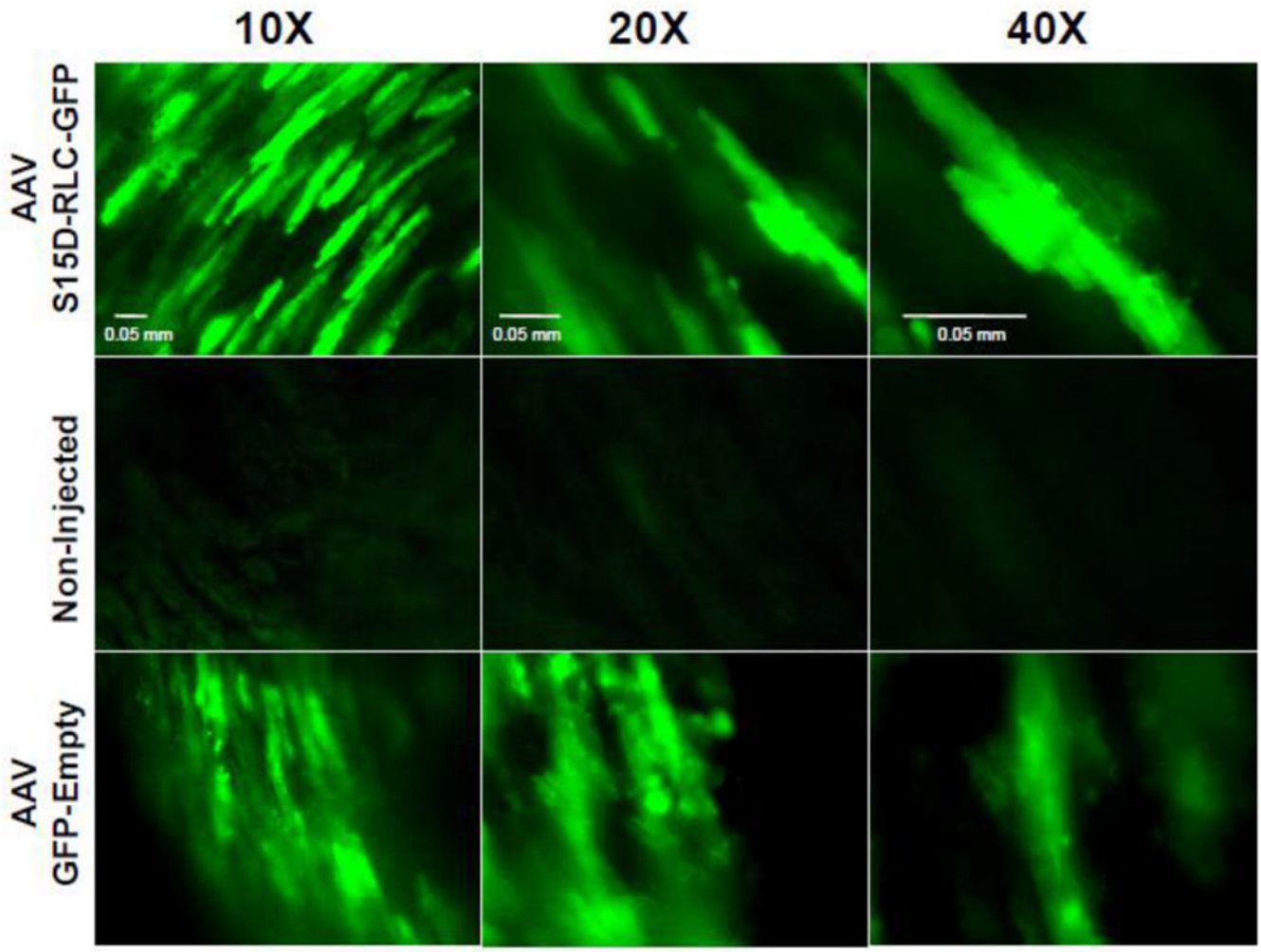

Figure 2.

Green fluorescent protein (GFP) expression within transgenic D166V HCM mice cardiomyocytes injected with AAV-huRLC-S15D-GFP (top) and AAV-GFP-empty vector (bottom) vs non-injected (middle) control. Exposure time for AAV-S15D-RLC-GFP/AAV-empty injected samples varied from 6.7-9.4 ms, while that for non-injected samples was 210 ms. Scale bars are 0.05 mm.

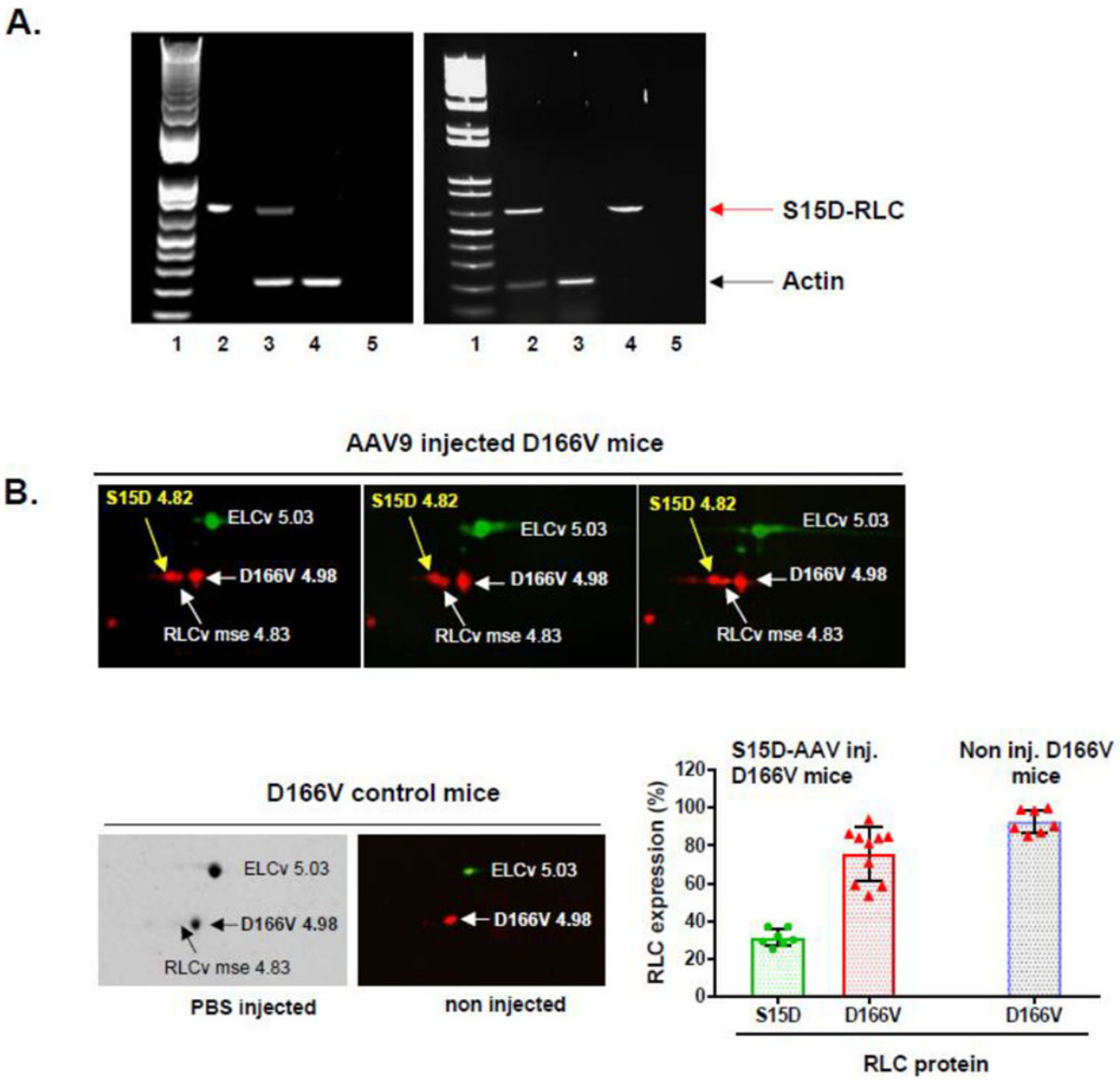

Figure 3.

A. PCR detection of AAV9 genome in the ventricles of non-transgenic (NTg) mice (left) and D166V HCM transgenic (Tg) mice (right) 7 days post injection. **Left PCR panel:** Lane1- DNA ladder, Lane2-vector positive ctr, Lane3-AAV9-S15D-RLC injected NTg mouse ventricle, Lane4-non-injected control NTg ventricle, Lane5-water ctr. **Right PCR panel:** Lane1- DNA ladder, Lane2-AAV9-S15D-RLC injected D166V ventricle, Lane3-non-injected D166V ventricle, Lane4-vector positive ctr, Lane5-water ctr. Red arrow – diagnostic band for AAV9-S15D-RLC genome; black arrow – actin (internal control). **B.** 2D-SDS-PAGE detection of human S15D-RLC in myosin from left ventricles of AAV9 injected (at 1.4×10^{11} vg) D166V (Western blots) vs PBS (Coomassie) or non-injected (Western blot)

D166V mice. Expression (E) of S15D was calculated using the formula E = S15D/(S15D +mseRLC+D166V). Average S15D-RLC expression in LV of AAV-injected D166V mice (by 2D-electrophoresis of n=7 samples from 5 animals) was 31±5% (Avg±SD). Average D166V RLC expression in D166V non-injected mice was 93±6% (n=7 samples from 2 animals) and 76±14 (n=10 samples from 6 animals) on AAV-S15D-RLC injected D166V mice.

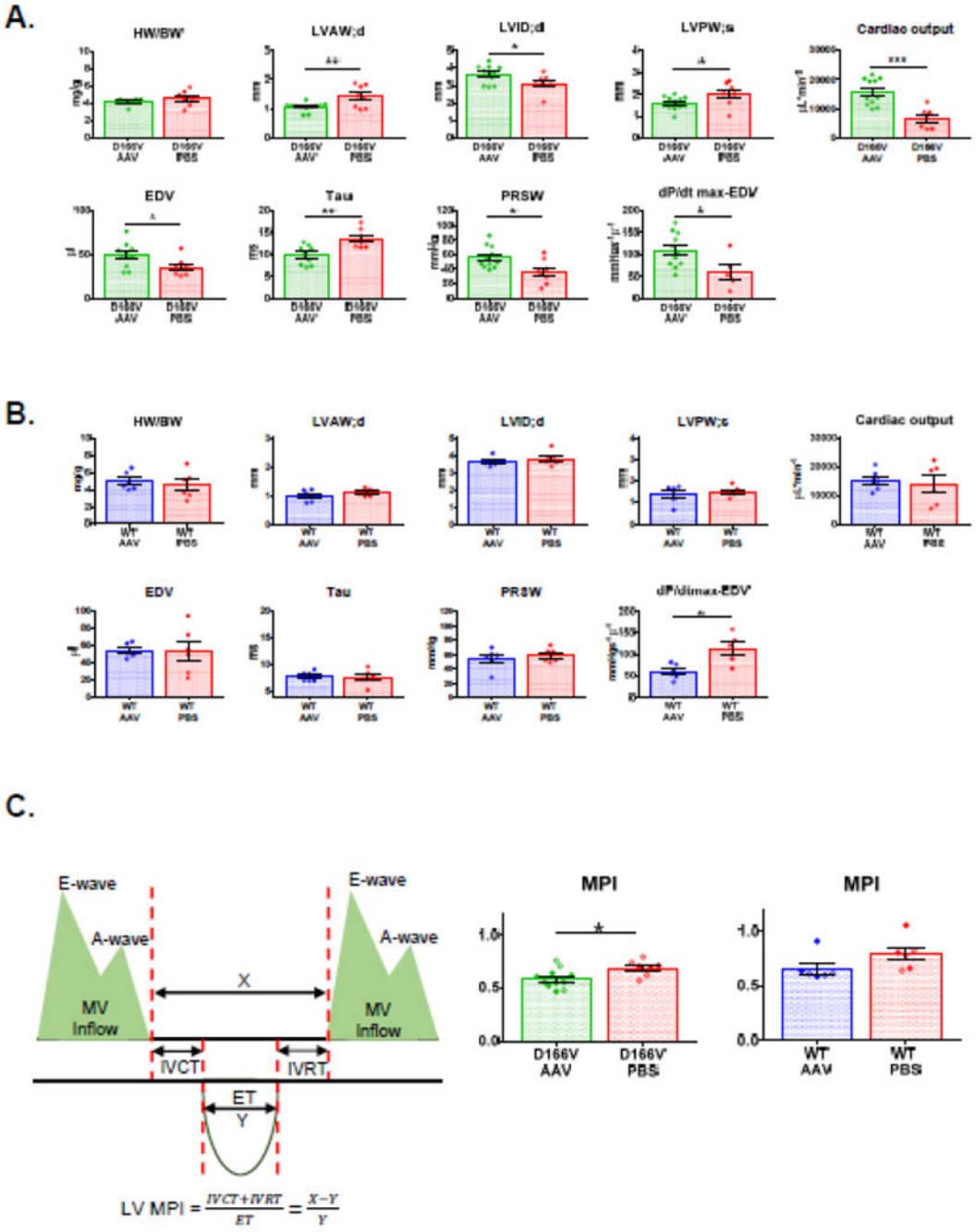

Figure 4.

In vivo characterization of D166V HCM **(A)** and WT **(B)** ~1-month post AAV/PBS systemic delivery. Abbreviations: HW/BW, Heart Weight to Body Weight ratio; LVAW;d, left ventricular anterior wall in diastole; LVID;d, left ventricular (LV) inner diameter in diastole; LVPW;s, LV posterior thickness in systole; Cardiac Output; EDV, end-diastolic volume; Tau, Relaxation constant; PRSW, Preload recruitable stroke work; dP/dtmax-EDV, peak rate of rise in LV pressure-end diastolic volume relationship. **C.** MPI, myocardial performance

index for D166V and WT mice ~l-month post AAV/PBS delivery. Data are mean ± SEM. *P<0.05, **P<0.01, and ***P<0.001, by Student's t-test.

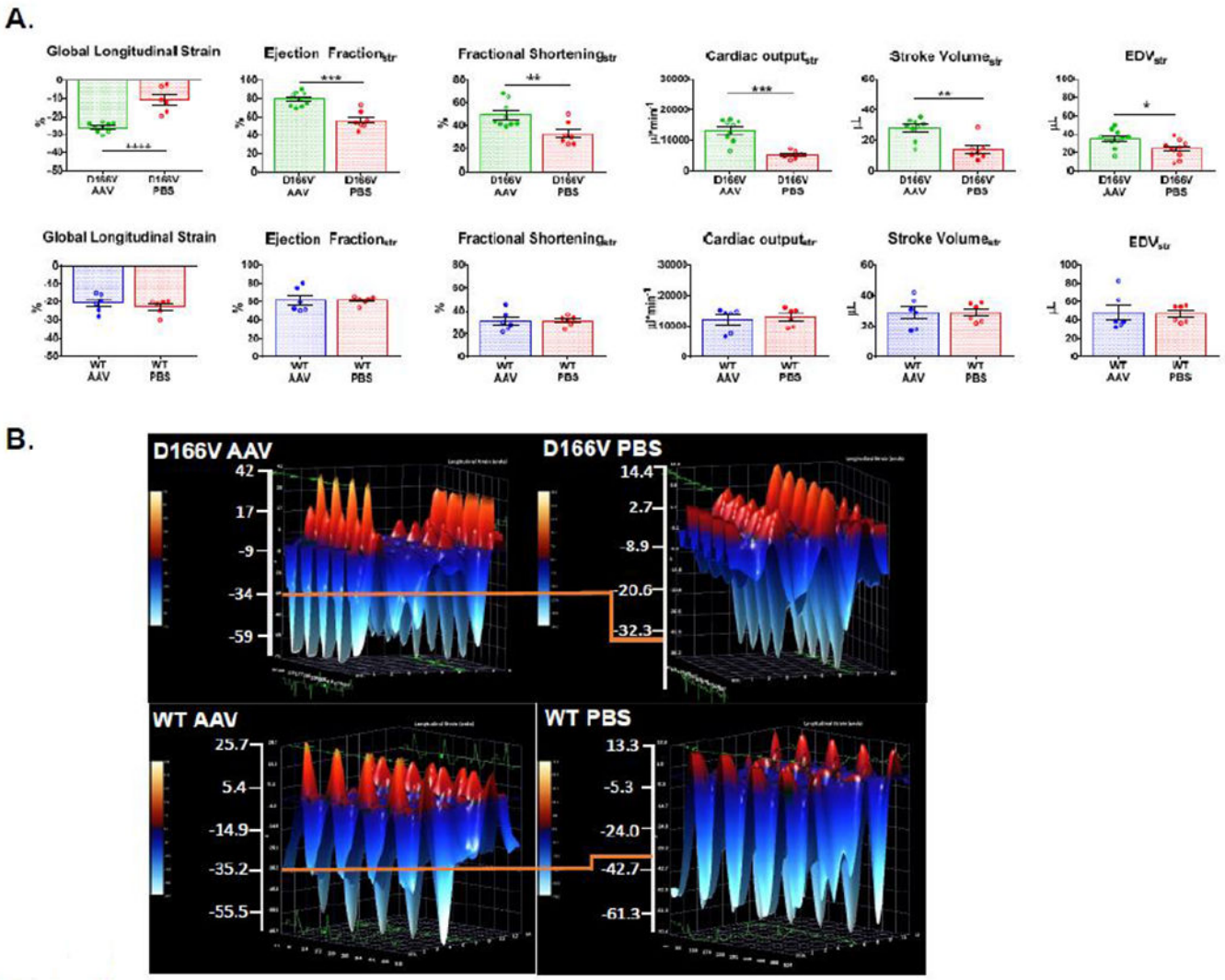

Figure 5.

A. Speckle-tracking based strain analysis in D166V (**top panel**) and WT (**bottom panel**) ~1 month post AAV/PBS delivery. Global longitudinal strain (GLS); Ejection Fraction$_{str}$; Fractional Shortening$_{str}$; Cardiac Output$_{str}$, Stroke Volume$_{str}$; EDV$_{str}$, End Diastolic Volume-*strain*. Data are mean ± SEM. *P<0.05, **P<0.01, ***P<0.001, ****P<0.0001, by Student's t-test. **B.** Representative three-dimensional longitudinal strain deformation images for D166V AAV/PBS (**top panel**) vs WT AAV/PBS (**bottom panel**) showing contraction (red, positive) and relaxation (blue, negative) over six LV segments during four consecutive cardiac cycles. The orange line has been added to aid comparison of the images' scale. Note significant improvement for strain parameters in D166V AAV animals compared to PBS. WT animals showed no significant differences.

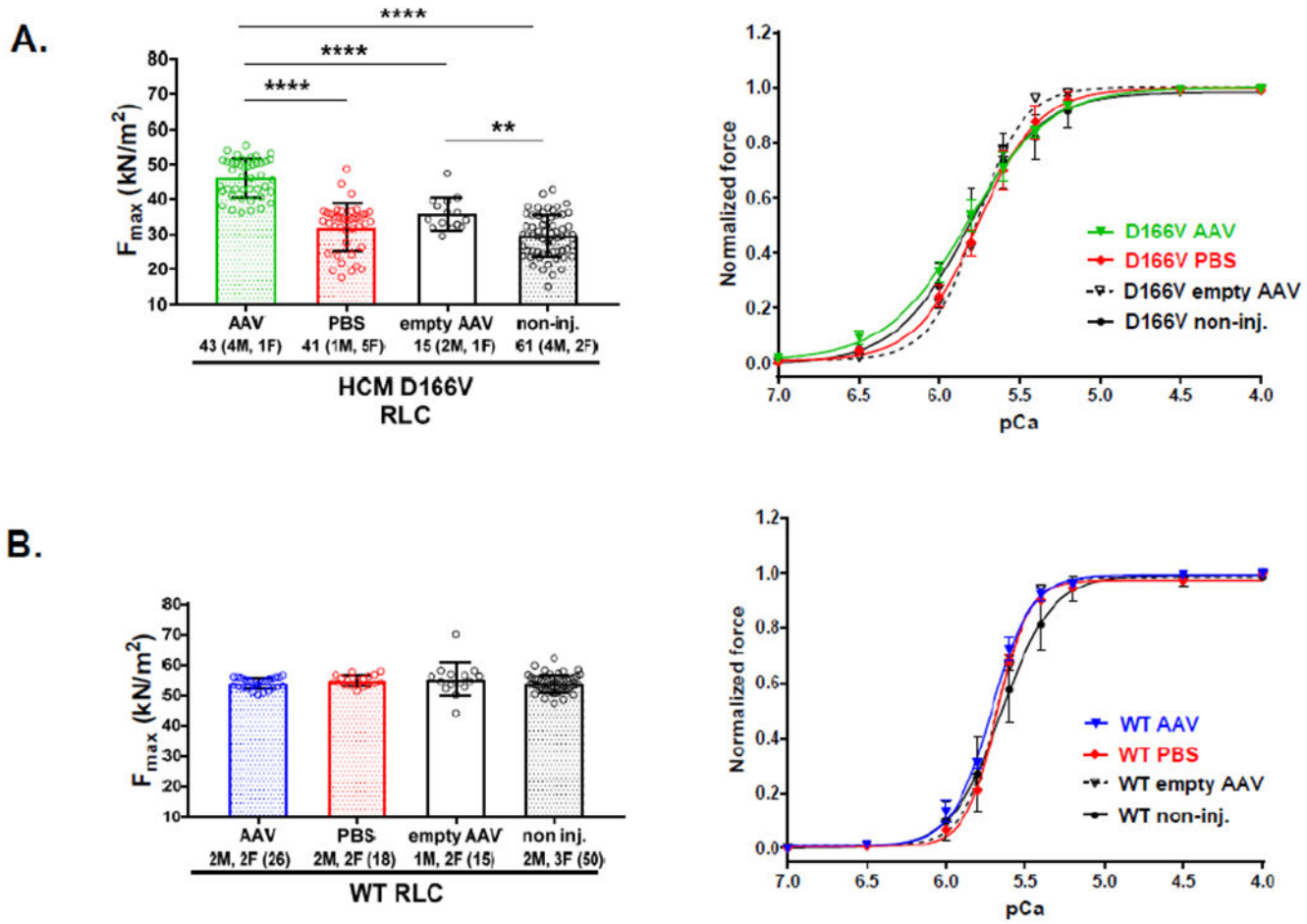

Figure 6.

Contractile function in skinned papillary muscle fibers from AAV-S15D-RLC, PBS and non-injected D166V **(A)** and WT **(B)** mice. Left panels show maximal tension at saturating (pCa 4) calcium concentrations per cross-section of muscle strip in kN/m^2. Right panels show the force-pCa relationship in D166V **(A)** and WT **(B)** mice. Values are means ± SD (standard deviation) for n = # fibers. **P<0.01 and ****P<0.0001, calculated by one-way ANOVA with Tukey's multiple comparison test. Note the improvement in steady-state force in AAV-S15D-RLC injected D166V mice compared with controls (PBS, AAV-empty and non-injected).

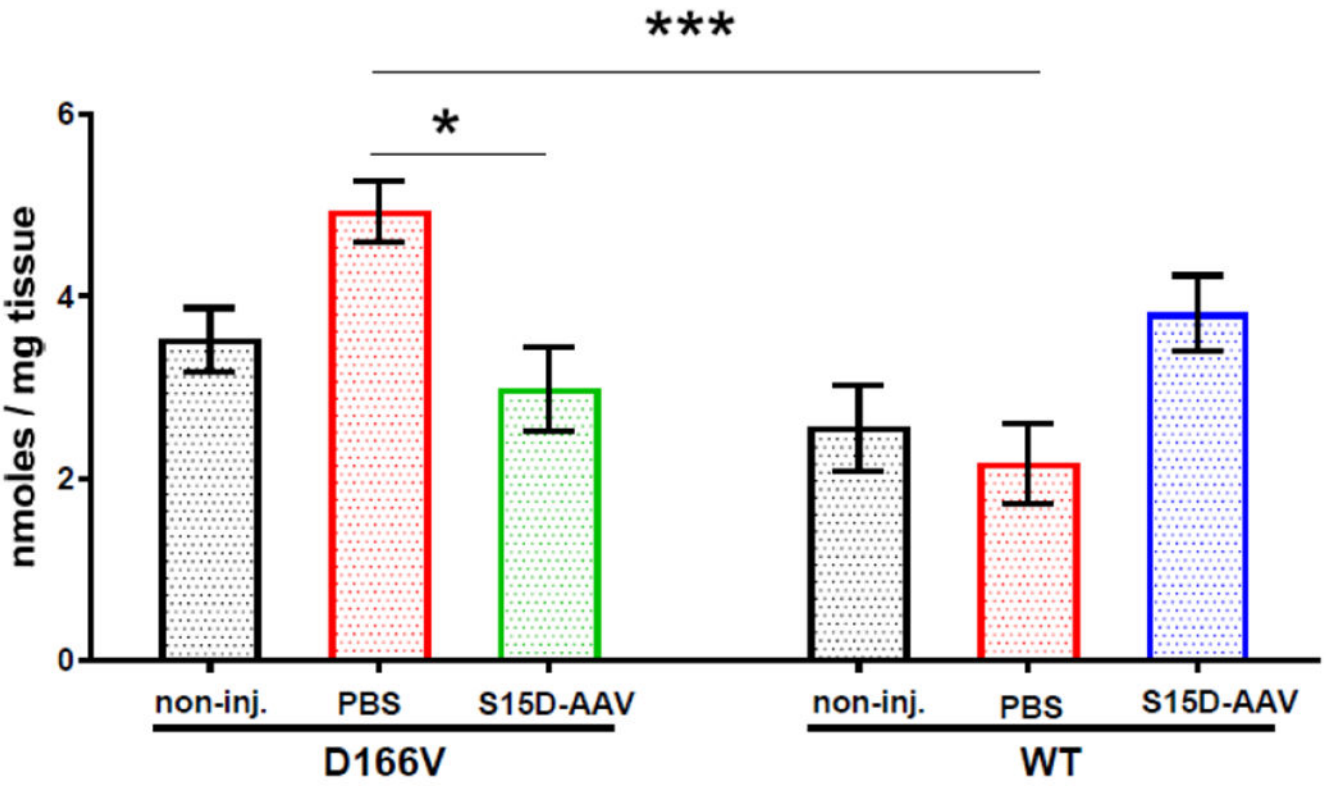

Figure 7.

Hydroxyproline (HOP) content in the hearts of AAV-S15D-RLC or PBS injected D166V and WT mice and non-injected controls was measured in female and male mice. 5-13 heart samples from 7-8 D166V and 3-6 WT animals were used. All assays were performed in triplicate. Data were plotted as mean ± SEM (n= number of samples). Comparisons among D166V and WT mice were performed using two-way ANOVA with Tukey's multiple test with *P<0.05, ***P<0.001.

Table 1.

Assessment of intact heart function in AAV vs PBS-injected D166V HCM and WT-RLC mice.

Echocardiography				
	D166V AAV	**D166V PBS**	**WT AAV**	**WT PBS**
No. of animals (n)	6F, 6M	5F, 3M	3F, 3M	3F, 3M
Heart/body (mg/g)	4.25±0.16	4.58±0.30	5.01±0.43	4.56±0.65
HR (bpm)	490±14	504±31	452±20	424±30
EF (%)	71±2	65±4	62±4	63±4
FS (%)	51±3	49±5	41±3	38±2
LVAW;d (mm)	1.06±0.04**	1.41±0.13	0.98±0.08	1.10±0.05
LVAW;s (mm)	1.78±0.09	2.04±0.16	1.57±0.09	1.65±0.05
LVID;d (mm)	3.64±0.14*	3.10±0.18	3.62±0.11	3.78±0.16
LVID;s (mm)	1.80±0.16	1.60±0.23	2.15±0.16	2.37±0.17
LVPW;d (mm)	0.96±0.04*	1.42±0.22	0.98±0.15	1.04±0.07
LVPW;s (mm)	1.60±0.09*	2.01±0.18	1.37±0.17	1.50±0.10
LV mass/corr (mg)	112.7±6.66	157.60±25.57	110.7±18.02	129.8±12.04
Doppler Analysis				
IVCT (ms)	13.61±1.16*	19.22±2.05	15.14±1.10*	21.84±2.53
IVRT (ms)	20.82±1.25	19.59±2.62	15.90±1.54	15.66±1.25
MV A (mm/s)	533±44	447±54	345±39	318±29
MV E (mm/s)	810±44**	547±82	655±34	645±46
MV E/A	1.36±0.06	1.35±0.14	1.89±0.15	1.98±0.16
MPI	0.59±0.03*	0.69±0.03	0.66±0.05	0.80±0.06
Invasive Hemodynamics				
SW (mmHg*µl)	2261±211***	918±211	2892±151	2448±445
CO (µl min^{-1})	15686±1383***	6653±1323	15243±1443	14006±2897
SV (µl)	31.27±2.48*	18.85±4.71	33.67±1.43	32.76±6.57
ESV (µl)	22.50±2.58	19.23±3.09	22.48±4.78	24.67±6.15
EDV (µl)	49.16±4.17*	35.70±3.59	53.80±3.25	53.92±11.02
Pes (mmHg)	86.08±2.98*	73.65±5.59	89.29±6.85	78.42±6.16
Ped (mmHg)	6.42±0.89	13.15±3.92	7.42±1.04	7.33±0.87
HR (bpm)	501±14	459±22	422±23	393±21
Ea (mmHg µl^{-1})	2.97±0.29*	5.34±1.00*	2.61±0.40	3.05±1.00
dP/dtmax (mmHg s^{-1})	8409±473	7441±998	6988±370	6426±663
−dP/dtmin (mmHg s^{-1})	5104±292	4961±729	7307±527	5825±595
Tau (ms)	9.93±0.66**	13.68±0.85*	7.89±0.37	7.77±0.59
ESPVR (mmHg µl^{-1})	2.56±0.45	2.42±0.48	2.29±0.41	2.74±0.34

Echocardiography				
	D166V AAV	**D166V PBS**	**WT AAV**	**WT PBS**
EDPVR (mmHg µl^{-1})	0.13±0.03	0.29±0.09	0.16±0.06	0.11±0.02
PRSW (mmHg)	56.04±4.57 *	36.36±5.85	55.15±5.77	58.50±3.92
dP/dtmax-EDV (mmHg s^{-1} µl^{-1})	110.7±11.75 *	60.93±17.49	60.20±7.09 *	113.5±16.00
Strain Analysis				
CO_{str} (µl min^{-1})	13344±1218 ***	5250±543	12217±1583	13000±1192
EF_{str} (%)	79±3 ***	56±4	62±5	62±2
FS_{str} (%)	49±4 **	33±4	31±4	32±2
EDV_{str} (µl)	35.24±2.82 *	24.10±3.02	48.13±8.14	46.68±3.74
SV_{str} (µl)	27.83±2.32 **	13.93±2.65	29.10±4.07	29.07±2.45
GLS (%)	−26.06±0.84 ****	−10.92±2.91	−20.63±2.05	−22.67±1.66

Data are mean ± SEM with *P<0.05, **P<0.01, ***P<0.001, and ****P<0.0001 depicting significance between AAV vs PBS treated mice, by Student's t-test.

Abbreviations: Heart weight/body weight in mg/g; Heart weigh/tibia length in mg/mm; HR, heart rate in beats per minute; EF%, ejection fraction; FS%, fraction of shortening; LVAW, left ventricular anterior wall; LVID, left ventricular inner diameter; LVPW, left ventricular posterior wall; d, diastolic; s, systolic; IVRT, isovolumetric relaxation time; IVCT, isovolumetric contraction time; MV E/A, mitral valve inflow -peak E-wave to A-wave velocity ratio; E, transmitral early peak velocity; E', early diastolic mitral annulus velocity; MPI, Myocardial Performance Index; CO, cardiac output; SW, stroke work; SV, stroke volume; ESV, end-systolic volume; EDV, end-diastolic volume; Pes, end-systolic pressure; Ped, end-diastolic pressure; Ea, arterial elastance; dP/dt max, peak rate for pressure rise; −dP/dtmin, peak rate for pressure decline; Tau, relaxation time constant; ESPVR, end-systolic PV relation (slope); EDPVR, end-diastolic PV relation (slope); PRSW, preload recruitable power stroke work; dP/dtmax-EDV, peak rate of rise in LV pressure-end diastolic volmne relationship; CO_{str}, Cardiac Output-*strain*; EF_{str}, Ejection Fraction-*strain*; FS_{str}, Fractional Shortening-*strain*; EDV_{str}, End Diastolic Volume-*strain*; SV_{str}, Stroke Volume-*strain*; GLS, global longitudinal strain.